Longitudinal electron scattering response functions of ^{3}H and ^{3}He

Victor D. Efros,[1,*] Winfried Leidemann,[1] Giuseppina Orlandini,[1] and Edward L. Tomusiak[2]
[1]*Dipartimento di Fisica, Università di Trento, and Istituto Nazionale di Fisica Nucleare, Gruppo Collegato di Trento, I-38050 Povo, Italy*
[2]*Department of Physics and Astronomy University of Victoria, Victoria, Canada BC V8P 1A1*
(Received 27 November 2003; published 1 April 2004)

Trinucleon longitudinal response functions $R_L(q,\omega)$ are calculated for q values up to 500 MeV/c. These are the first calculations beyond the threshold region in which both three-nucleon ($3N$) and Coulomb forces are fully included. We employ two realistic NN potentials (configuration space BonnA, AV18) and two $3N$ potentials (UrbanaIX, Tucson-Melborne). Complete final state interactions are taken into account via the Lorentz integral transform technique. We study relativistic corrections arising from first-order corrections to the nuclear charge operator. In addition the reference frame dependence due to our nonrelativistic framework is investigated. For $q \leqslant 350$ MeV/c we find that $3N$ forces give effects of between 5 % and 10 % in the peak region and of 15 % in the threshold region at the lowest considered momentum transfer ($q=174$ MeV/c), while the dependence on other theoretical ingredients is small. At $q \geqslant 400$ MeV/c relativistic corrections to the charge operator and effects of frame dependence, especially for large ω, become more important. In comparison with experimental data there is generally a rather good agreement. Exceptions are the responses at excitation energies close to threshold, where there exists a large discrepancy with experiment at higher q. In the ^{3}He case one finds a much improved agreement with experiment both in the peak region and in the low-q–low-ω region if $3N$ forces are included. However in comparison with the existing data for ^{3}H the inclusion of $3N$ forces appears to have the opposite effect in the peak region.

DOI: 10.1103/PhysRevC.69.044001 PACS number(s): 25.30.Fj, 21.45.+v, 21.30.−x, 31.15.Ja

I. INTRODUCTION

Inclusive electron scattering can provide detailed information on the transition charge and current densities in nuclei. In the one-photon exchange approximation the cross section for this process is given by [1]

$$\frac{d^2\sigma}{d\Omega\, d\omega} = \sigma_M \left[\frac{q_\mu^4}{q^4} R_L(q,\omega) + \left(\frac{q_\mu^2}{2q^2} + \tan^2\frac{\theta}{2} \right) R_T(q,\omega) \right], \tag{1}$$

where R_L and R_T are the longitudinal and transverse response functions, respectively, ω is the electron energy loss, q is the magnitude of the electron momentum transfer, θ is the electron scattering angle, and $q_\mu^2 = q^2 - \omega^2$. Experimental data for both R_L and R_T are available for a variety of energy and momentum transfers. However because of our nonrelativistic treatment of the nuclear dynamics we restrict our attention to momentum transfers $q \leqslant 500$ MeV/c and energy transfers $\omega \leqslant 300$ MeV. Data covering various regions in this range are given for both ^{3}H and ^{3}He by Retzlaff *et al.* [2], Dow *et al.* [3], Marchand *et al.* [4], and Morgenstern [5].

The theoretical treatment of these response functions requires the ability to accurately include transitions to the continuum. Techniques for doing this with realistic NN potentials have only been developed and implemented during the past ten years. These include both Faddeev and Lorentz integral transform (LIT) methods [6,9–12]. For the $3N$ photodisintegration total cross sections results obtained with the LIT [13] and Faddeev techniques are compared in Ref. [14]. In the work of Viviani *et al.* [15] expansion techniques were applied to solving the ground-state and continuum wave equations, but the calculation was restricted to a ^{3}He near threshold region where only the two-body breakup occurs. Previous to the above references Faddeev calculations of trinucleon response functions were published by Meijgaard and Tjon [16] in 1992 using the s-wave Malfliet-Tjon potential MT-I/III [17]. Apart from how the quantum mechanics is done there are major differences in physics input between the longitudinal and transverse responses. Whereas the nonrelativistic longitudinal response requires only a charge operator and nucleon form factors, the transverse response requires exchange currents in addition to single-nucleon currents and nucleon form factors. It is clear that if a given nuclear interaction cannot describe the longitudinal response then it would be pointless to attempt a calculation of the transverse response. In particular if one inquires into the effect of three-body forces in nuclei it would appear natural to first investigate their impact on the longitudinal response. Otherwise, through a calculation of R_T, it would be difficult to disentangle the effects of three-body forces from exchange current effects. Further as shown in Ref. [10] the longitudinal response appears in general insensitive to the realistic NN force model thus removing a possible source of ambiguity when comparing the effects of different three-body force models on $R_L(q,\omega)$.

Our paper is organized as follows. Section II lists the two- and three-nucleon forces considered here and details the nuclear charge operator. In Sec. III the calculation of the response via the LIT method is explained. Effects of the various theoretical ingredients contributing to the longitudinal response are discussed in Sec. IV, where also a compari-

*Permanent address: Russian Research Centre "Kurchatov Institute," 123182 Moscow, Russia.

TABLE I. ^{3}H ground-state properties with AV18+UrbIX, AV18+TM′, and BonnRA+TM′ potentials for binding energy (EB), point charge radius (r), and probabilities of total orbital angular momentum components in percentage; results for ^{3}He are also given, but for AV18+UrbIX only.

	^{3}H(AV18+UrbIX)	^{3}H(AV18+TM′)	^{3}H(BonnRA+TM′)	^{3}He(AV18+UrbIX)
EB (MeV)	8.47	8.47	8.47	7.73
r(fm)	1.588	1.589	1.587	1.772
S' wave	1.05	1.05	1.02	1.23
P wave	0.13	0.13	0.08	0.13
D wave	9.27	9.23	7.23	9.22

son with experimental data is made. Conclusions are drawn in Sec. V.

II. NUCLEAR FORCES AND CHARGE OPERATOR

The function R_L represents the response of the nucleus through the nuclear charge operator ρ and is given by

$$R_L(q,\omega) = \overline{\sum_{M_0}} \int\!\!\!\!\!\!\diagup df \langle\Psi_0|\rho^\dagger(\mathbf{q},\omega)|\Psi_f\rangle\langle\Psi_f|\rho(\mathbf{q},\omega)|\Psi_0\rangle \times \delta(E_f - E_0 + q^2/(2M_T) - \omega). \quad (2)$$

Here M_T is the mass of the target nucleus, Ψ_0 and Ψ_f denote the ground and final states, respectively, while E_0 and E_f are energies pertaining to them,

$$(H - E_0)\Psi_0 = 0, \quad (H - E_f)\Psi_f = 0, \quad (3)$$

where H is the nuclear nonrelativistic Hamiltonian. The above quantities $\Psi_{0,f}$ and H are internal quantities in the hadronic c.m. frame. The integration (summation) goes over all final states belonging to the same energy E_f, and M_0 is the projection of the ground-state angular momentum.

The Hamiltonian includes the kinetic energy terms, the NN and $3N$ force terms, and the proton Coulomb interaction term in the ^{3}He case. The ground state Ψ_0 is calculated via an expansion in basis functions which are correlated sums of products of hyperradial functions, hyperspherical harmonics, and spin-isospin functions. In the present work three models of the NN force are used: the realistic AV18 [18] and configuration space BonnA (herein referred to as BonnRA) [19] models, and the s-wave MT−I/III potential. We consider two $3N$ force models, the UrbIX [20] and the TM′ [21], in the combinations AV18+UrbIX, AV18+TM′(Λ =3.358 fm^{-1}), and BonnRA+TM′(Λ=2.835 fm^{-1}). As indicated the TM′ cutoff parameter Λ is different in the AV18 and BonnRA combinations in order to properly fix the ^{3}H binding energy in each case. Table I lists our results for ground-state properties for the above potential combinations containing the $3N$ force. We should mention that the UrbIX $3N$ force is fitted to obtain the ^{3}H binding energy of 8.48 MeV. The ^{3}He-^{3}H mass difference is not yet completely understood even if the AV18 electromagnetic corrections, which we do not include, are considered [22]. For the cases with the TM′ $3N$ force we choose the cutoff Λ such that we obtain exactly the same ^{3}H binding energy as in our calculation with AV18+UrbIX.

As nuclear charge operator we take the following one-body operator:

$$\rho(\mathbf{q},\omega) = \sum_{j=1}^{A} \rho_j^{nr}(\mathbf{q},\omega) + \rho_j^{rc}(\mathbf{q},\omega), \quad (4)$$

where

$$\rho_j^{nr}(\mathbf{q},\omega) = \hat{e}_j e^{i\mathbf{q}\cdot\mathbf{r}_j}, \quad (5)$$

$$\rho_j^{rc}(\mathbf{q},\omega) = -\frac{q^2}{8M^2}\hat{e}_j e^{i\mathbf{q}\cdot\mathbf{r}_j} - i\frac{\hat{e}_j - \hat{\mu}_j}{4M^2}\vec{\sigma}_j\cdot(\mathbf{q}\times\mathbf{p}_j)e^{i\mathbf{q}\cdot\mathbf{r}_j}, \quad (6)$$

$$\hat{e}_j = G_E^p(q_\mu^2)\frac{1+\tau_{z,j}}{2} + G_E^n(q_\mu^2)\frac{1-\tau_{z,j}}{2} \equiv \frac{1}{2}[G_E^S(q_\mu^2) + G_E^V(q_\mu^2)\tau_{z,j}], \quad (7)$$

$$\hat{\mu}_j = G_M^p(q_\mu^2)\frac{1+\tau_{z,j}}{2} + G_M^n(q_\mu^2)\frac{1-\tau_{z,j}}{2}. \quad (8)$$

Here $\mathbf{r}$, $\mathbf{p}$, $\vec{\sigma}$, and $\vec{\tau}$ are the nucleon position, momentum, and spin and isospin operators, M is the nucleon mass, and $G_{E,M}^{p,n}$ are the nucleon Sachs form factors. The two terms in Eq. (6) proportional to M^{-2} are the Darwin-Foldy (DF) and spin-orbit (SO) relativistic corrections to the main operator (5), see, e.g., Refs. [1,23]. We refer to the main operator (5) as the nonrelativistic one although the dependence of nucleon form factors on q_μ^2 does not allow a nonrelativistic interpretation.

In this work we mainly use the well-known dipole fit for the proton electric form factor, while the neutron electric form factor is taken from Ref. [24]. The nucleon electric form factors have not yet been determined with extremely high precision. The neutron form factor, however, is small and the fit of Ref. [24] has also been confirmed in recent experiments (see, e.g., Ref. [25]). More important for the reliability of our R_L calculation is a check of the result due to uncertainties in the much larger proton electric form factor. Thus we also use the fit from Ref. [26]. In the momentum range up to q=500 MeV/c the two different form factor fits describe the experimental data with similar quality, but nevertheless lead to somewhat different results. In case of the SO term we adopt the usual although recently controversial

[31] approximation $G_M^{p,n}(q_\mu^2)=\mu_{p,n}G_E^p(q_\mu^2)$ in Eq. (8), $\mu_{p,n}$ being proton and neutron magnetic momenta. We have checked by using a wide range of form factor models that for the kinematics considered here deviations from this scaling law would not lead to any visible effect in our various figures.

For the calculation of R_L it is convenient to rewrite the operator ρ in terms of the isoscalar and isovector charge nucleon form factors from Eq. (7),

$$\rho(\mathbf{q},\omega)=G_E^S(q_\mu^2)\rho_s(\mathbf{q})+G_E^V(q_\mu^2)\rho_v(\mathbf{q}). \tag{9}$$

The inclusion of relativistic corrections for the one-body charge operator only is not completely consistent. In fact there exist additional relativistic effects: a wave function boost (as done in Refs. [29,30] for the $d(e,e')$ reaction) and additional two-body terms in the charge operator (as done in Ref. [15] for the low-energy two-body breakup channel of the ^{3}He(e,e') reaction). In our case there are two reasons why we include the relativistic corrections to the one-body charge operator.

(i) At higher q they lead to an important reduction of the R_L quasielastic peak height. As illustrated in Ref. [30] such a reduction is confirmed if boost corrections are included. Moreover, the frame dependence of the response functions is studied in Ref. [29] where it is shown that in the Breit frame boost corrections are negligibly small for the quasielastic peak region (different kinematics are not shown). We believe that one has a similar frame dependence of boost corrections also for the electromagnetic response of the three-nucleon systems. Thus we will make the comparison with experimental data taking R_L from a Breit frame calculation with a subsequent transformation into the R_L lab frame result (see discussion of Fig. 5).

(ii) They enable us to make a direct comparison of our results with those of Ref. [15]. Since realistic few-body calculations are rather complicated it is of great importance to have these kinds of checks.

III. CALCULATION OF RESPONSE

We calculate $R_L(q,\omega)$ by the LIT method as described in Refs. [6,7]. The technique is, however, directly applicable only when the transition operator does not depend on ω. To separate out the ω dependence of the transition operator we use Eq. (9) to represent the response function (2) as

$$R_L(q,\omega)=[G_E^S(q_\mu^2)]^2\,\mathcal{R}_s+G_E^S(q_\mu^2)G_E^V(q_\mu^2)\mathcal{R}_{sv}+[G_E^V(q_\mu^2)]^2\mathcal{R}_v, \tag{10}$$

where $\mathcal{R}_s$ and $\mathcal{R}_v$ are the responses which emerge if $\rho_s(\mathbf{q})$ and $\rho_v(\mathbf{q})$ are taken as transition operators, and the quantity $\mathcal{R}_{sv}$ is the mixed response,

$$\mathcal{R}_{sv}(q,\omega)=\sum_{M_0}\int\!\!\!\!\!\!\diagup df[\langle\Psi_0|\rho_s^\dagger(\mathbf{q})|f\rangle\langle f|\rho_v(\mathbf{q})|\Psi_0\rangle+\langle\Psi_0|\rho_v^\dagger(\mathbf{q})|f\rangle \times\langle f|\rho_s(\mathbf{q})|\Psi_0\rangle]\delta(E_f-E_0+q^2/(2M_T)-\omega). \tag{11}$$

To calculate the subsidiary responses entering Eq. (10) with the LIT method one can solve the inhomogeneous equations

$$(H-E_0-\sigma)\tilde{\Psi}_s(\sigma)=\rho_s\Psi_0,\quad (H-E_0-\sigma)\tilde{\Psi}_v(\sigma)=\rho_v\Psi_0 \tag{12}$$

for a set of complex σ values and then form the scalar products $\langle\tilde{\Psi}_s(\sigma)|\tilde{\Psi}_s(\sigma)\rangle$, $\langle\tilde{\Psi}_v(\sigma)|\tilde{\Psi}_v(\sigma)\rangle$, and $\langle\tilde{\Psi}_s(\sigma)|\tilde{\Psi}_s(\sigma)\rangle$. These scalar products represent integral transforms with Lorentzian kernels, e.g., one has

$$\langle\tilde{\Psi}_s(\sigma)|\tilde{\Psi}_s(\sigma)\rangle=\frac{\mathcal{F}_s^2(q)}{|\sigma|^2}+\int_{\omega_{th}}^{\infty}d\omega\frac{\mathcal{R}_s(q,\omega)}{(\omega-\omega_{el}-\sigma)(\omega-\omega_{el}-\sigma^*)}. \tag{13}$$

Here ω_{th} is the threshold for the inelastic energy transfer and $\mathcal{F}_s(q)$ is the isoscalar elastic form factor with the nucleon form factor $G_E^S(q_\mu^2)$ divided out. The elastic contribution to $\mathcal{R}_s$ equals $\mathcal{F}_s^2(q)\delta(\omega-\omega_{el})$, where $\omega_{el}=q^2/(2M_T)$. From the inversion of such integral transforms one then obtains the response functions $\mathcal{R}_s$, $\mathcal{R}_v$, and $\mathcal{R}_{sv}$.

In previous work [7] equations similar to those in Eq. (12) were solved numerically in order to calculate the above mentioned scalar products $\langle\tilde{\Psi}_i(\sigma)|\tilde{\Psi}_j(\sigma)\rangle$. An alternative and computationally more efficient way of calculating the transform is by a direct evaluation of the scalar products via the Lanczos technique [28]. Thus we use this method in our calculation.

As for Ψ_0 we perform expansions in terms of basis functions $|\mu\rangle$ which are correlated sums of products of hyperradial functions, hyperspherical harmonics, and spin-isospin functions. The first Lanczos vector is given by

$$|\varphi_0\rangle=\frac{|\Psi\rangle}{\sqrt{\langle\Psi|\Psi\rangle}} \tag{14}$$

with

$$|\Psi\rangle=g^{-1}\hat{\rho}|\Psi_0\rangle, \tag{15}$$

where g^{-1} denotes the inverse of the norm matrix g with matrix elements $g_{\mu\nu}=\langle\mu|\nu\rangle$. One then applies the following relations for $n\geqslant 0$ recursively:

$$b_{n+1}|\varphi_{n+1}\rangle=g^{-1}H|\varphi_n\rangle-a_n|\varphi_n\rangle-b_n|\varphi_{n-1}\rangle, \tag{16}$$

with

$$\langle\varphi_n|\varphi_n\rangle=1,\quad a_n=\langle\varphi_n|H|\varphi_n\rangle,\quad b_0=0. \tag{17}$$

The transform can then be written as a continuous fraction,

$$\langle\tilde{\Psi}|\tilde{\Psi}\rangle=\frac{2i}{\sigma-\sigma^*}Im\frac{\langle\Psi|\Psi\rangle}{(z-a_0)-\dfrac{b_1^2}{(z-a_1)-\dfrac{b_2^2}{(z-a_2)-b_3^2\cdots}}}. \tag{18}$$

with $z=\sigma+E_0$.

The functions $\tilde{\Psi}$ possess definite values of parity P, angular momenta J, and magnetic quantum numbers M_J. Various Lanczos sets are separated with respect to these quantum numbers. Multipole expansions of the operators ρ_s and ρ_v are performed, which allows elimination of dependencies on M_J and on the ground-state angular momentum projection M_0. In our case there exists only one multipole ℓ compatible with a given J and P value. Indeed, one has $J=\ell\pm 1/2$ and parity equal to $(-1)^{\ell}$.

In order to calculate Eq. (18) we perform, as already mentioned, expansions of the Lanczos states $|\varphi_n\rangle$ over basis functions. Let ρ and $\{\Omega\}$ be the hyperradius and hyperangles defined as usual. The basis functions are products of hyperradial functions $R_n(\rho)$ and spin-isospin-hyperangular functions. The latter functions include hyperspherical harmonics (HH) depending on $\{\Omega\}$ and functions of spin and isospin variables. We use HH belonging to given permutational symmetry types which are obtained via application of the corresponding symmetrization operators to HH of the type $Y^{l_1 l_2}_{KLM_L}$. Here K is the grand-angular momentum, L and M_L are the total orbital momentum and its projection, and l_1 and l_2 are the orbital momenta associated with the relative motion of a given pair of particles and the relative motion of the third particle with respect to the pair. The spin-isospin functions possess given spin S, isospin T, and permutational symmetry. The HH obtained are coupled to the spin-isospin functions of conjugated permutational symmetry types to get functions antisymmetric with respect to permutations of nucleons and also to get a given total momentum. Thus our basis functions have given J, M_J, K, L, S, T values, given parity equal to $(-1)^K$, and given type of symmetry with respect to permutations of spatial, or spin-isospin, variables. In order to accelerate the convergence of the HH expansion a spin and isospin dependent correlation operator is applied to the basis functions (see Ref. [13] for details). Matrix elements are calculated analytically with respect to three Euler angles determining the orientation of the system as a whole, and the remaining three-dimensional integrations are done numerically.

For any value of J one has four separate systems according to isospin and parity, thus, in case of a maximal value of $J=21/2$ one has 44 separate systems. Rather many basis functions are retained to achieve convergence, and a selection of basis HH has been done to reduce their net numbers in the calculation. The selection is based upon the property [27] that the uncorrelated symmetrized basis HH obtained in the above mentioned way from the subset of HH $Y^{l_1 l_2}_{KLM_L}$ with only small l_1 and small l_2 suffice to provide a predominant contribution to bound state wave functions. We have found that in practice this property is also valid for our correlated HH and for the case of our inhomogeneous equations. At the same time, the selection depended on L, K, J values and symmetry types of HH as well. Typically we include about 150 HH states for any system. We should also mention that we dropped in the final calculation the isospin mixing of the AV18 potential after having checked that it leads only to very small effects on the response functions (much below 1%).

The mixed response (11) is calculated as

TABLE II. ^{3}H Coulomb sum rule for AV18, AV18+UrbIX, and MT−I/III Potentials (we estimate to have an error of 0.005 in calculating the sum rules).

q (MeV/c)	$J_{\max}$	AV18	AV18+UrbIX	MT-I/III
250	$\frac{15}{2}$	0.998	0.999	1.000
300	$\frac{15}{2}$	0.993	0.994	
350	$\frac{21}{2}$	0.992	0.993	
400	$\frac{21}{2}$	1.003	0.998	
450	$\frac{21}{2}$	0.998	0.999	
500	$\frac{21}{2}$	0.977	0.977	0.994

$$\mathcal{R}_{sv} = \mathcal{R}_{s+v} - \mathcal{R}_s - \mathcal{R}_v, \tag{19}$$

where $\mathcal{R}_{s+v}$ is the response, which emerges from the scalar product $\langle\tilde{\Psi}_{s+v}(\sigma)|\tilde{\Psi}_{s+v}(\sigma)\rangle$, and $\tilde{\Psi}_{s+v}(\sigma)$ is obtained if $\rho_s+\rho_v$, instead of ρ_s or ρ_v, is taken as the transition operator in Eq. (12).

IV. RESULTS AND DISCUSSION

Before showing detailed results of our calculations it is necessary to address the question of convergence with respect to the maximum angular momentum J_{max} retained in our calculation. This requires some measure of convergence. In this connection we consider here the ^{3}H Coulomb sum rule results computed for the case $G_E^S=G_E^V=1$. The sum rule reads in this case

$$\int_{\omega_{th}}^{\infty} R_L(q,\omega)d\omega + \mathcal{F}^2(q) = 1. \tag{20}$$

Here $\mathcal{F}(q)$ is the elastic form factor at $G_E^S=G_E^V=1$. Since in the case considered a single proton interacts with the electromagnetic field, Eq. (20) does not contain the nucleon charge correlation contribution and is valid for any q. It is clear that larger q values require the expansion to include larger values of J. Table II shows the results of using $J_{max}=15/2$ for the $q=250$, and 300 MeV/c cases and $J_{max}=21/2$ for the $q=350-500$ MeV/c cases. One notes that the lower q sum rules are nearly fully converged while the 500 MeV/c case still requires about 2 % more strength. Although this could be improved by increasing J_{max} we consider the convergence tolerable for the present investigation. Table II also demonstrates that the convergence is faster for the simple MT−I/III potential as compared to the realistic potential models.

In Fig. 1 we illustrate the dependence of R_L on the NN potential. The results with the two realistic potentials, BonnRA and AV18, are very similar at $q=500$ MeV/c, but exhibit somewhat stronger differences for the quasielastic peak height at $q=250$ MeV/c. With the semirealistic MT−I/III potential one observes a rather similar picture for $q=250$ MeV/c as with the realistic potentials, whereas at $q=500$ MeV/c a greater peak height and considerably less high-energy strength than for the realistic potentials is found.

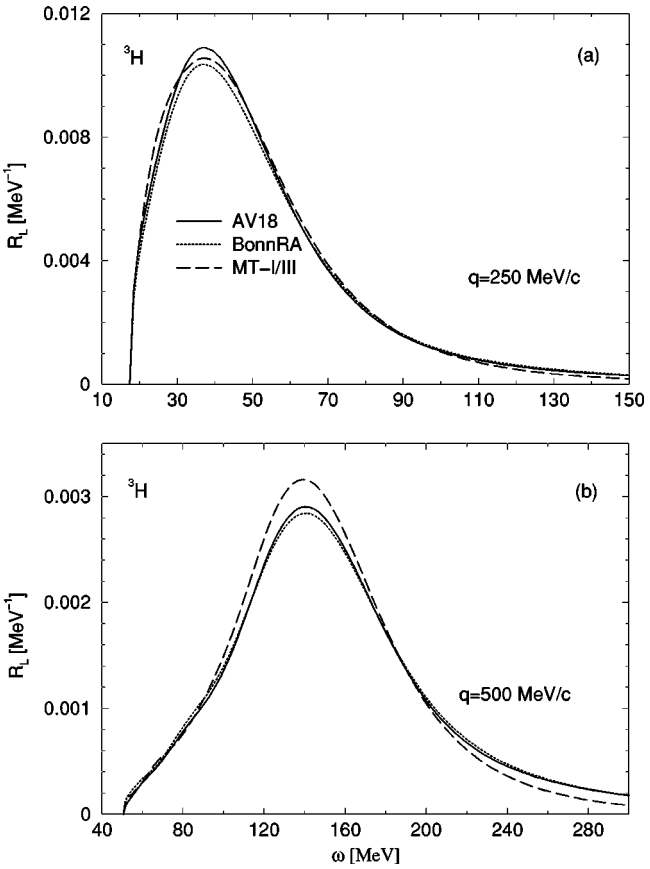

FIG. 1. *NN* potential model dependence of triton $R_L^{LAB}(q_{LAB},\omega_{LAB})$ at $q_{LAB}=250$ (a) and 500 (b) MeV/c (charge operator, nonrelativistic plus DF term): AV18 (solid), BonnRA (dotted), and MT-I/III (dashed).

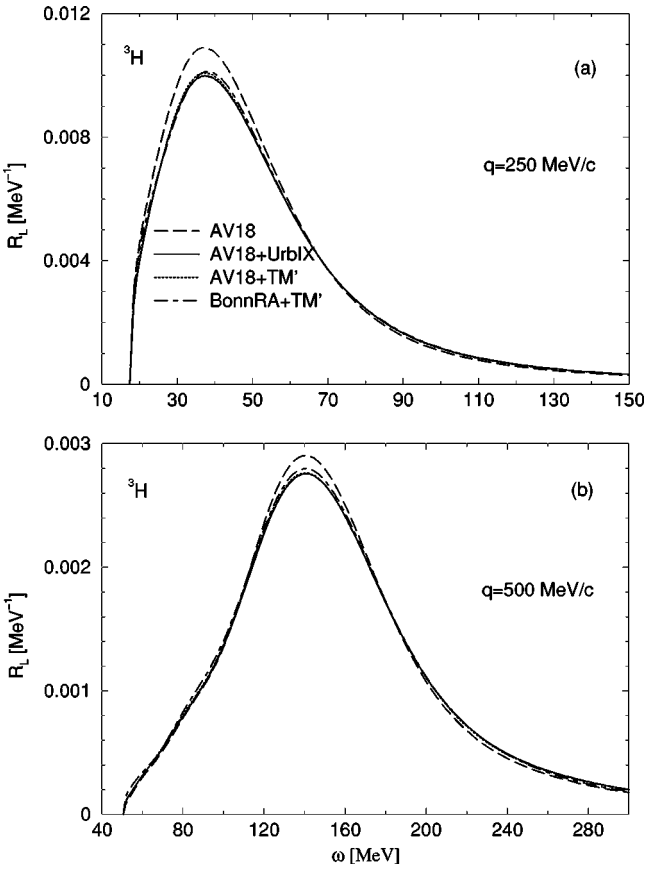

FIG. 2. Effect of 3*N* force on triton $R_L^{LAB}(q_{LAB},\omega_{LAB})$ at $q_{LAB}=250$ (a) and 500 (b) MeV/c (charge operator, nonrelativistic plus DF term): AV18 (dashed), AV18+UrbIX (solid), AV18+TM′ (dotted), and BonnRA+TM′ (dash dotted).

In Fig. 2 we show the 3*N* force effect. It is seen that it decreases the peak height and enhances the high-energy tail. At lower momentum transfer the reduction of the peak height is more pronounced. Comparing the three cases, where a 3*N* force is included, one finds only rather small differences among them except for the low-energy range at $q=500$ MeV/c as will be seen next in Fig. 3.

In order to study the low-energy behavior better, in Fig. 3 we illustrate the nuclear force model dependence of the triton R_L close to threshold at three momentum transfers covered also by the data of Ref. [2]. In this figure R_L is shown as a function of E_x, the relative kinetic energy of the outgoing three nucleons. At $q=174$ MeV/c there is a rather strong decrease of R_L due to the 3*N* force. The reduction becomes considerably smaller at $q=324$ MeV/c, and at $q=487$ MeV/c the 3*N* force leads to an opposite effect, namely, a moderate increase. From the comparison of the cases AV18+UrbIX and AV18+TM′ it becomes clear that the 3*N* force model dependence for all the three momentum transfers is very small. The only evident potential model dependence is found at the highest q, where the case BonnRA+TM′ exhibits considerably more strength than the other cases with inclusion of 3*N* force.

In Fig. 4 we show the effect of the relativistic corrections on R_L. One sees that the SO term leads only to rather small contributions, while the DF term is more important. It occurs that separate contributions from the SO term are not so small, only their net sum proves to be very small. This probably means that in the inclusive case we have an effect of averaging out due to the spin dependence of the SO operator. Because of the smallness of the SO contribution we have neglected it in most of the following cases. In Fig. 4 we also show R_L results, where a different proton electric form factor [26] is taken. At $q=250$ MeV/c the different proton form factor leads to a similar small reduction as the DF contribution, while at $q=500$ MeV/c there is an almost 5 % reduction of R_L. In the results which follow we will always use the dipole nucleon form factors. However as seen here there will be uncertainties in R_L at higher q values due to uncertainties in the proton electric form factor.

Next we would like to check the frame dependence of our calculation. To this end we calculate R_L also in the Breit (B) frame and the so-called antilab (AL) frame. In the AL frame the virtual photon and initial target nucleus have momenta $\mathbf{q}_{AL}$ and $-\mathbf{q}_{AL}$, respectively, whereas the total momentum of the final three-nucleon state is equal to zero. Note that in the lab frame one has the opposite case: the target nucleus in the initial state is at rest and the total momentum of the final three-nucleon state is equal to $\mathbf{q}$. Finally, in the Breit frame one has total momenta of initial and final hadron states equal to $-\mathbf{q}_B/2$ and $\mathbf{q}_B/2$, respectively, while the photon four-momentum is $(\omega_B,\mathbf{q}_B)$. Formally there are no differences be-

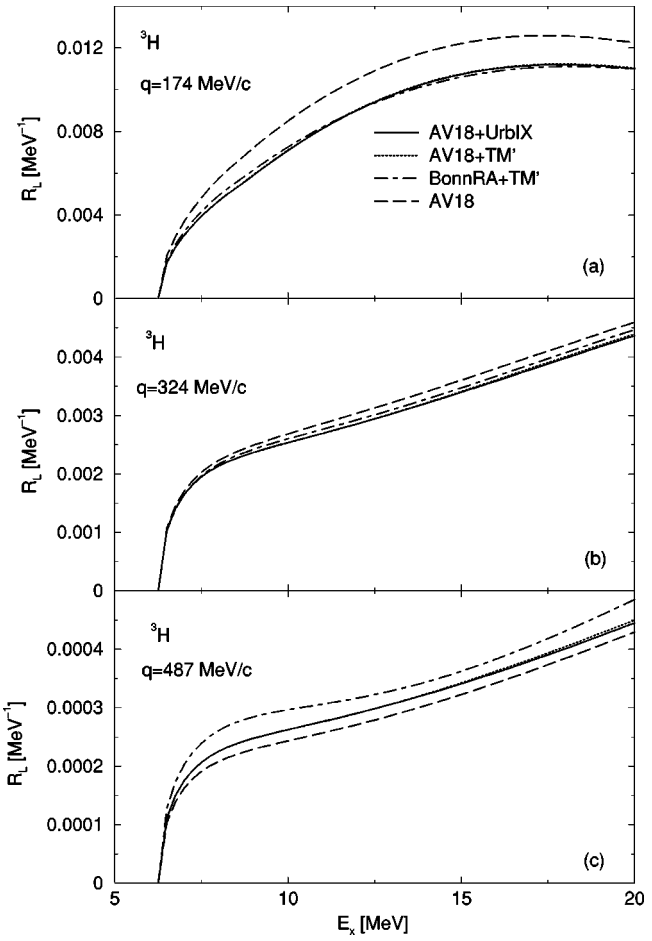

FIG. 3. Effect of 3*N* force on low-energy triton $R_L^{LAB}(q_{LAB},E_x,)$ at q_{LAB}174 (a), 324 (b), and 487 (c) MeV/c (charge operator, nonrelativistic plus DF term): AV18 (dashed), AV18+UrbIX (solid), AV18+TM′ (dotted), and BonnRA+TM′ (dash dotted).

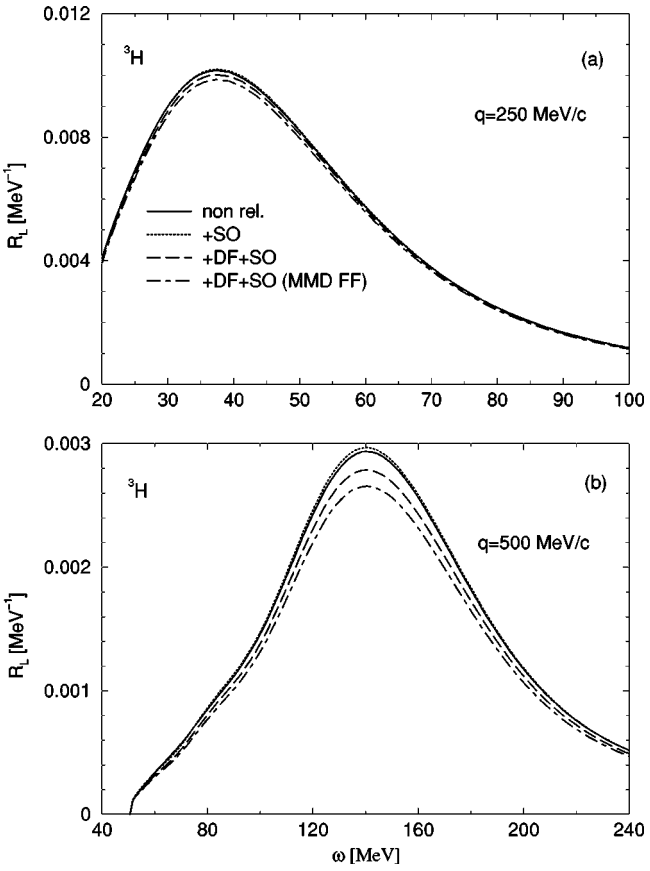

FIG. 4. Effect of relativistic contributions and nucleon form factor dependence for triton $R_L^{LAB}(q_{LAB},\omega_{LAB})$ at q_{LAB}=250 (a) and 500 (b) MeV/c (potential model, AV18+UrbIX): nonrelativistic charge operator (solid), additional inclusion of SO term (dotted), and total result with further inclusion of DW term (dashed), all three cases with neutron electric form factor from [24] and dipole fit for the other three nucleon form factors. Total result also with proton electric form factor from Ref. [26] and other form factors as above (dash dotted).

tween the calculations in the various frames. One obtains a response function which has the arguments ω and q of the given frame, i.e., $R_L^{LAB}(q_{LAB},\omega_{LAB})$, $R_L^{AL}(q_{AL},\omega_{AL})$, and $R_L^{B}(q_B,\omega_B)$. For a comparison of the results we transform $R_L^{AL}(q_{AL},\omega_{AL})$ and $R_L^{B}(q_B,\omega_B)$ into $R_L^{LAB(AL)}(q_{LAB},\omega_{LAB})$ and $R_L^{LAB(B)}(q_{LAB},\omega_{LAB})$, respectively. To this end we use that the various reference frames are connected via Lorentz boosts and thus ω_{AL}, q_{AL}, ω_B, and q_B can be expressed through ω_{LAB} and q_{LAB}. However in order to obtain an R_L in the lab frame from R_L's in AL and Breit frames it is not sufficient to transform the relative arguments of ω and q into the corresponding lab frame arguments. In addition one has

$$R_L^{LAB(frame)} = \frac{q_{LAB}^2}{q_{frame}^2} R_L^{frame}, \tag{21}$$

where "*frame*" stands for AL or Breit. The origin of the additional factor is the following. The cross section of Eq. (1) contains three separate pieces, namely, σ_M, a part regarding the electron (e.g., $q_\mu^4/q^4 \equiv V_L^{LAB}$) and a hadronic part (e.g., R_L). The latter two originate from a reduction of a product of leptonic and hadronic Lorentz tensors [1]. The product of these two tensors forms a Lorentz scalar and thus is frame independent. One can show that for the longitudinal part of the cross section of Eq. (1) one has [29]

$$V_L^{LAB} = \frac{q_{frame}^2}{q_{LAB}^2} V_L^{frame} \tag{22}$$

and thus Lorentz invariance requires the additional factor in Eq. (21).

In Fig. 5 we compare the longitudinal response functions of the various frames. At q=250 MeV/c differences are rather small, in particular between Breit and AL frame results. Except for the threshold region there is not such a similar good agreement at q=500 MeV/c. In the quasielastic peak there are rather pronounced differences: $R_L^{LAB(AL)}$ is about 7% and $R_L^{LAB(B)}$ about 4% higher than R_L^{LAB}, their peak positions are shifted by about 6 (AL) and 5 MeV (B) towards lower energies. In a consistent relativistic theory one would of course have identical results and thus the obtained

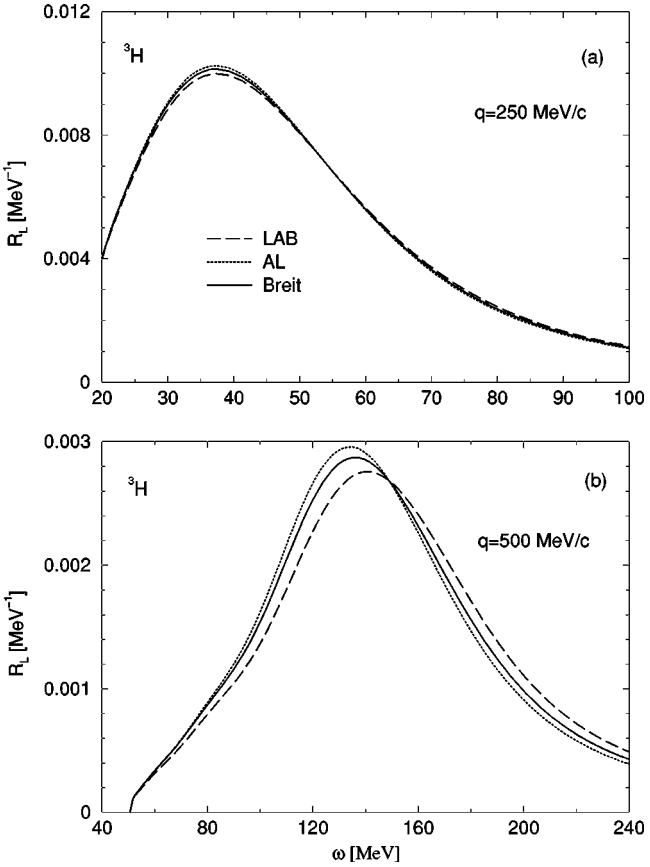

FIG. 5. Frame dependence of triton $R_L(q_{LAB},\omega_{LAB})$ at q_{LAB} =250 (a) and 500 (b) MeV/c (potential model, AV18+UrbIX; charge operator, nonrelativistic plus DF term): R_L^{LAB} (dashed), $R_L^{LAB(AL)}$ (dotted), and $R_L^{LAB(B)}$ (solid).

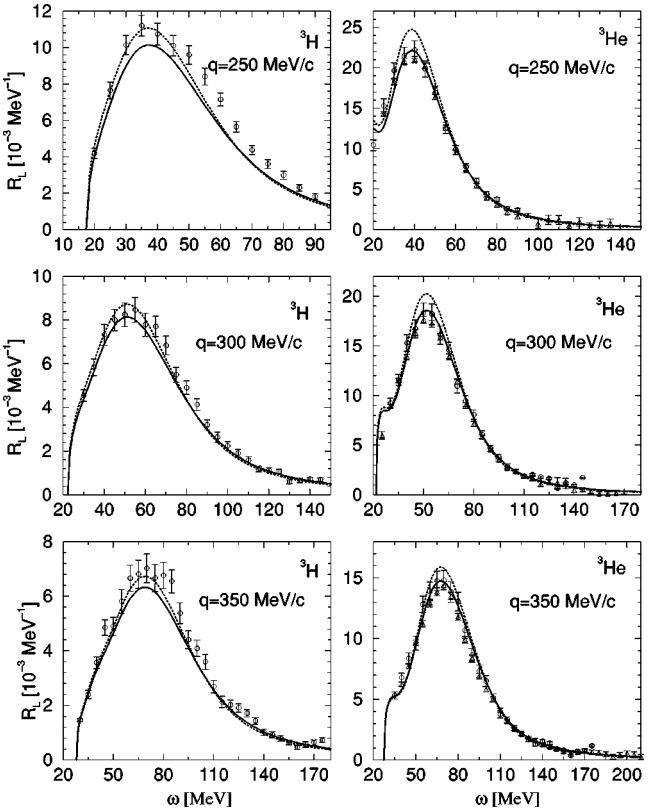

FIG. 6. Comparison of theoretical and experimental $R_L^{LAB(B)}(q_{LAB},\omega_{LAB})$ at q_{LAB} as indicated in figure for ^{3}H (left) and ^{3}He (right) (charge operator, nonrelativistic plus DF term): AV18 +UrbIX potentials (solid) and AV18 potential (dotted); experimental data from Ref. [3] (circles) and Refs. [4,5] (triangles).

differences point to a relativistic inconsistency in the calculation.

As mentioned before Beck *et al.* [29] studied the electromagnetic response functions in deuteron electrodisintegration in the quasielastic region. They have shown that an inclusion of boost effects on the hadron wave functions leads essentially to the same results for the various reference frames discussed here. In addition they have found that boost corrections are almost vanishing in the Breit frame. We believe that also in the three-nucleon electrodisintegration one probably has a similar picture with a strong cancellation of boost effects in the Breit frame. Therefore we will take the $R_L^{LAB(B)}$ results in comparison with quasielastic experimental data.

A comparison of the ^{3}H and ^{3}He theoretical longitudinal response functions with experimental data of Refs. [3–5] is shown in Fig. 6 at q=250, 300, and 350 MeV/c. In the peak region one does not find a clear picture, since there is a better agreement once with the 3N force (^{3}He) and once without the 3N force (^{3}H). Except for the triton case at q =250 MeV/c one observes rather similar theoretical and experimental results for the high-energy tail. At higher energies the size of the experimental errors is larger than the effect of the 3N force, thus nothing can be said there about an improvement of the theoretical result with the 3N force.

In Fig. 7 we show equivalent results as in Fig. 6 but at the higher momentum transfers of 400, 450, and 500 MeV/c. Also here one finds a better agreement with experimental data without the 3N force in case of ^{3}H and with the 3N force in case of ^{3}He. It is worthwhile to note that for all six cases of Fig. 7 one has a good agreement of theoretical and experimental peak positions. Concerning the low- and high-energy tails one has a rather good agreement between theory and experiment.

Next we turn to a comparison of the triton low-energy longitudinal response functions with the experimental data of Ref. [2]. In Fig. 8 we show the R_L of ^{3}H at various q. Since the R_L frame dependence is very small close to threshold we illustrate directly the results from a lab frame calculation. For the lower two momentum transfers there is a rather good agreement between experiment and theory, but the size of the experimental error is too large to draw definite conclusions about possible improvements due to the 3N force. At q =487 MeV/c the picture is different: the theoretical response functions are larger than the experimental one, in particular very close to threshold. It is also evident that the effect of the 3N force moves the calculated R_L even further away from the data.

In Fig. 9 we show a similar comparison with experimental data as in Fig. 8 but for the R_L of ^{3}He. Again one finds a rather good agreement between theory and experiment for

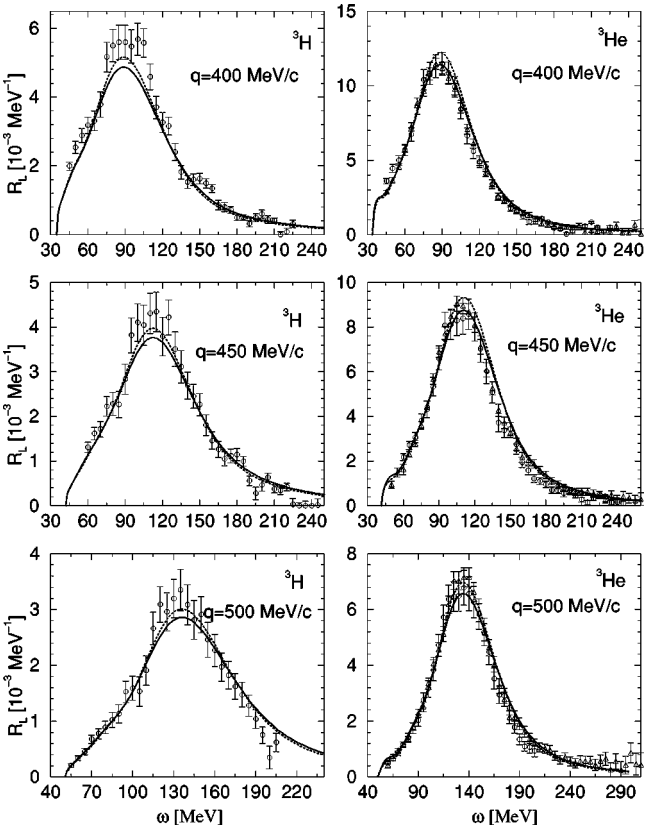

FIG. 7. As Fig. 6 but for different momentum transfers q_{LAB} as indicated in figure.

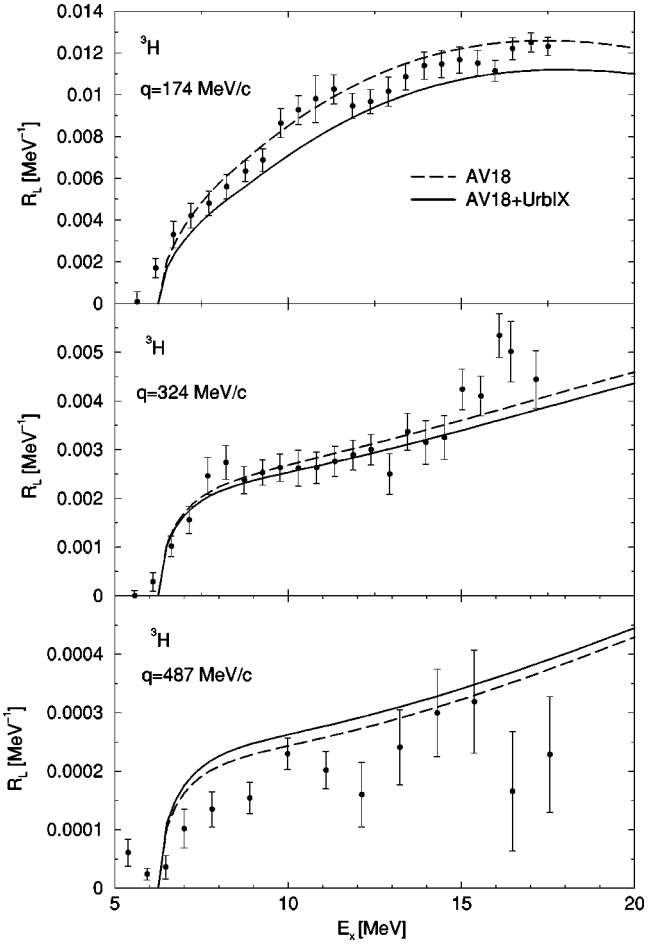

FIG. 8. Comparison of theoretical and experimental $R_L^{LAB}(q_{LAB},E_x)$ for ^{3}H at q_{LAB} as indicated in figure (charge operator, nonrelativistic plus DF term): AV18+UrbIX potentials (solid) and AV18 potential (dashed); experimental data from Ref. [2].

the two lower q's, but contrary to the triton case here the 3N force is important for this agreement at $q=174$ MeV/c. Also for the highest momentum transfer one finds a similar picture as for the triton case, namely, a large overestimation of the experimental data by the theoretical response functions and also an increase of R_L due to the 3N force.

In Fig. 9 we also illustrate theoretical results from Ref. [15]. It is an approach to calculating responses, which is entirely different from ours. The calculation [15] has been carried out with the AV18+UrbIX potentials, relativistic DF- and SO-terms have been included, and the same nucleon form factors as by us have been used (dipole fit, neutron electric form factor from Ref. [24]). In order to have a clean comparison of the two different calculations, we also take into account the SO term for our result with AV18 and UrbIX, though its effect is also very small here. For the two higher momentum transfers there is a rather good agreement between both calculations. Some differences are visible at $q=174$ MeV/c, but the difference between the two calculations is still considerably smaller than the experimental error bars.

The rather large discrepancy between theory and experiment of the low-energy R_L at $q=487$ MeV/c requires further theoretical and experimental investigations. We should mention that in the calculation of Ref. [15] relativistic two-body charge operators were also considered. Although they were not sufficient to give agreement with experiment, they did diminish the discrepancy by about a factor of 2. Concerning the nucleon form factors one could only obtain a small reduction (about 5 %) using the fit of Ref. [26]. In addition the potential model dependence should be further studied. In the discussion of Fig. 3 we have already mentioned a rather strong potential model dependence of the low-energy R_L at $q=487$ MeV/c. Therefore it would be interesting to consider other modern realistic *NN* potentials in addition to the AV18 and BonnRA models used here.

V. CONCLUSIONS

In the following we give a brief summary of our work. The trinucleon longitudinal response function $R_L(q,\omega)$ is calculated with realistic *NN* interactions and 3N and Coulomb forces for a variety of kinematical settings that include momentum transfers q between 174 and 500 MeV/c and wide ranges of energy transfers ω. The results are fully convergent. The calculations are performed via the Lorentz integral transform method.

As *NN* interaction we use a modern realistic (AV18), a realistic (BonnRA), and also a semirealistic (MT−I/III) potential model. Two models (UrbIX, TM′) of the 3N force are employed. The treatment of the trinucleon dynamics is com-

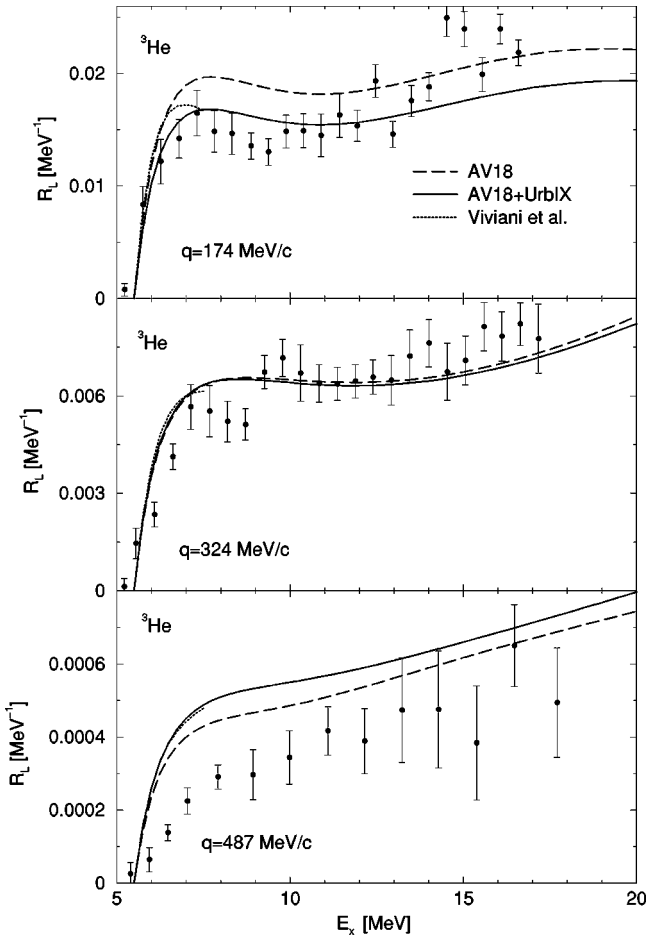

FIG. 9. Comparison of theoretical and experimental $R_L^{LAB}(q_{LAB},E_x)$ for ^{3}He at q_{LAB} as indicated in figure (charge operator, nonrelativistic plus DF and SO terms): AV18+UrbIX potentials (solid) and AV18 potential, but without inclusion of SO term (dashed); experimental data from Ref. [2]. Theoretical result from Ref. [15] (dotted) with AV18+UrbIX potentials and same charge operators as in our AV18+UrbIX case.

pletely nonrelativistic. Nonetheless we apply a minimal check on the uncertainties related to this. For this purpose we evaluate R_L in three different reference frames, namely, in lab, antilab, and Breit frames. For the charge operator we take the leading relativistic corrections into account (Darwin-Foldy and spin-orbit terms).

In general we find a rather small *NN* potential model dependence, but in some cases there are also larger effects. These include the height of the quasielastic peak at lower q and the threshold behavior at higher q. The effect of the 3*N* force is typically between 5% and 10%, but reaches up to 15% for the low-energy response at low q. The dependence on the 3*N* force model is very small for all considered cases.

Concerning the relativistic contributions to the charge operator, our inclusive case shows negligible effects due to the spin-orbit term, while the DF term leads to non-negligible effects at higher q. With respect to the R_L calculation in the various reference frames, we observe a non-negligible frame dependence at higher q, except for the threshold region. In order to restore a more consistent relativistic behavior one would need to consider additional relativistic effects. Similar results have been found in $d(e,e')$ and it is shown that additional boost corrections lead to a much better agreement among the various frame results [29]. In the same work it is also shown that boost effects are negligible in the Breit frame. We assume a similar behavior also in trinucleon electrodisintegration. Thus we compare the R_L calculated in the Breit frame with experimental data.

The comparison of our results with experimental data is generally rather satisfying for all considered momentum transfers, in particular for the R_L of ^{3}He. The experimental data, however, are in most cases not precise enough to draw definite conclusions about the 3*N* force effect. A nice exception is the ^{3}He low-energy response, where a 3*N* force proves to be necessary to obtain agreement with experiment. In addition for the ^{3}He quasielastic peak heights at $q \leqslant 400$ MeV/c three-nucleon forces considerably improve the agreement with experiment. At higher-q and low-ω values one finds a considerably higher R_L response in theory than in experiment.

Last but not the least we would like to mention that at very low energies, i.e., up to the three-body breakup threshold, we can compare our results with those of Ref. [15]. We find quite a good agreement. The differences which do show up at very low-q are still smaller than the experimental error bars.

ACKNOWLEDGMENTS

We thank K. Dow for sending us easily plottable data from her experiment described in Ref. [3] and M. Viviani for giving us his theoretical results [15]. One of us (W.L.) thanks H. Arenhövel for a discussion concerning the reference frame problems. Acknowledgments of financial support are given to the Russian Ministry of Industry and Science, Grant No. NS-1885.2003.2 (V.D.E.) and to the National Science and Engineering Research Council of Canada (E.L.T.).

[1] T. deForest, Jr., and J. D. Walecka, Adv. Phys. **15**, 1 (1994).
[2] G. A. Retzlaff *et al.*, Phys. Rev. C **49**, 1263 (1994).
[3] K. Dow *et al.*, Phys. Rev. Lett. **61**, 1706 (1988).
[4] C. Marchand *et al.*, Phys. Lett. **153B**, 29 (1985).
[5] J. Morgenstern (private communication).
[6] V. D. Efros, W. Leidemann, and G. Orlandini, Phys. Lett. B **338**, 130 (1994).
[7] V. D. Efros, W. Leidemann, and G. Orlandini, Phys. Rev. Lett. **78**, 432 (1997).
[8] W. Leidemann, V. D. Efros, G. Orlandini, and E. L. Tomusiak, Fiz. B **8**, 135 (1999).
[9] S. Martinelli, H. Kamada, G. Orlandini, and W. Glöckle, Phys.

Rev. C **52**, 1778 (1995).
[10] J. Golak, H. Witała, H. Kamada, D. Hüber, S. Ishikawa, and W. Glöckle, Phys. Rev. C **52**, 1216 (1995); S. Ishikawa, H. Kamada, W. Glöckle, J. Golak, and H. Witała, Phys. Lett. B **339**, 293 (1994).
[11] W. Glöckle, H. Kamada, J. Golak, H. Witała, S. Ishikawa, and D. Hüber, *Proceeding of Electronuclear Physics with Internal Targets and the Blast Detector*, (MIT, Cambridge, MA, 1998).
[12] W. Leidemann, Few-Body Syst., Suppl. **14**, 313 (2003).
[13] V. D. Efros, W. Leidemann, G. Orlandini, and E. L. Tomusiak, Phys. Lett. B **484**, 223 (2000); Nucl. Phys. **A689**, 421c (2001).
[14] J. Golak, R. Skibiński, W. Glöckle, H. Kamada, A. Nogga, H. Witała, V. D. Efros, W. Leidemann, G. Orlandini, and E. L. Tomusiak, Nucl. Phys. **A707**, 365 (2002).
[15] M. Viviani, A. Kievsky, L. E. Marcucci, S. Rosati, and R. Schiavilla, Phys. Rev. C **61**, 064001 (2000).
[16] E. van Meijgaard and J. A. Tjon, Phys. Rev. C **45**, 1463 (1992).
[17] R. A. Malfliet and J. A. Tjon, Nucl. Phys. **A127**, 161 (1969).
[18] R. B. Wiringa, V. G. J. Stoks, and R. Schiavilla, Phys. Rev. C **51**, 38 (1995).
[19] R. Machleidt, Adv. Nucl. Phys. **19**, 189 (1989).
[20] B. S. Pudliner, V. R. Pandharipande, J. Carlson, S. C. Pieper, and R. B. Wiringa, Phys. Rev. C **56**, 1720 (1997).
[21] S. A. Coon, M. D. Scadron, P. C. McNamee, B. R. Barrett, D. W. E. Blatt, and B. H. J. McKellar, Nucl. Phys. **A317**, 242 (1979); S. A. Coon and W. Glöckle, Phys. Rev. C **23**, 1790 (1981); S. A. Coon (private communication) giving the most recent parameters as $a' = -1.35\mu^{-1}$, $b = -2.86\mu^{-3}$, and $d = -0.64\mu^{-3}$.
[22] A. Nogga, A. Kievsky, H. Kamada, W. Glöckle, L. E. Marcucci, S. Rosati, and M. Viviani, Phys. Rev. C **67**, 034004 (2003).
[23] J. M. Friar, Ann. Phys. (N.Y.) **81**, 332 (1973).
[24] S. Galster, H. Klein, J. Moritz, K. H. Schmidt, D. Wegener, and J. Bleckwenn, Nucl. Phys. **B32**, 221 (1971).
[25] J. Bermuth *et al.*, Phys. Lett. B **564**, 199 (2003).
[26] P. Mergell, U.-G. Meissner, and D. Drechsel, Nucl. Phys. **A596**, 367 (1996).
[27] V. D. Efros, Sov. J. Nucl. Phys. **13**, 758 (1972).
[28] M. A. Marchisio, N. Barnea, W. Leidemann, and G. Orlandini, Few-Body Syst. **33**, 259 (2003).
[29] G. Beck and H. Arenhövel, Few-Body Syst. **13**, 165 (1992); G. Beck, T. Wilbois, and H. Arenhövel, *ibid.* **17**, 91 (1994).
[30] T. Wilbois, G. Beck, and H. Arenhövel, Few-Body Syst., Suppl. **15**, 39 (1993).
[31] R. Segel, Bull. Am. Phys. Soc. **48**, 8 (2003).